ANL-8016

ANL-8016

EVALUATION OF A CLASS OF METHODS FOR BOUNDING STEADY-STATE CREEP DEFORMATION

John J. Carey and Richard A. Valentin

BASE TECHNOLOGY

U of C-AUA-USAEC

ARGONNE NATIONAL LABORATORY, ARGONNE, ILLINOIS

Prepared for the U.S. ATOMIC ENERGY COMMISSION
Division of Reactor Research and Development
under Contract W-31-109-Eng-38

MASTER

DISCLAIMER

Printed in the United States of America
Available from
National Technical Information Service
U.S. Department of Commerce
5285 Port Royal Road
Springfield, Virginia 22151
Price: Printed Copy $4.00; Microfiche $1.45

ANL-8016
LMFBR Structural Materials
and Design Engineering
(UC-79h)

ARGONNE NATIONAL LABORATORY
9700 South Cass Avenue
Argonne, Illinois 60439

EVALUATION OF A CLASS OF METHODS FOR BOUNDING STEADY-STATE CREEP DEFORMATION

by

John J. Carey and Richard A. Valentin

Components Technology Division

February 1974

THIS PAGE
WAS INTENTIONALLY
LEFT BLANK

TABLE OF CONTENTS

LIST OF FIGURES

LIST OF FIGURES

TABLE

EVALUATION OF A CLASS OF METHODS FOR BOUNDING STEADY-STATE CREEP DEFORMATION

by

John J. Carey and Richard A. Valentin

ABSTRACT

This report evaluates theorems, due to Martin and Palmer, for bounding steady-state creep deformation. Upper and lower bounds on the displacement rate at any point on the surface of a structure undergoing steady creep are determined in terms of arbitrary equilibrated stress distributions, and arbitrary consistent velocity fields. The theorems are applied to several problems for which exact solutions are known in order to assess the accuracy of the bounds based on a particular stress or velocity field. A procedure utilizing elastic finite-element analysis to compute the bounds is described, together with an example.

I. INTRODUCTION

Bounding theorems for structural deformation can provide a useful tool for design purposes--provided the theorems yield reasonably accurate results, are easily applied to complex structures with arbitrary load history, and do not require extensive computation. For situations in which structural deformations must be limited, such theorems can be used to establish deformation bounds and thus possibly avoid the use of expensive finite-element analysis.

This report is concerned with an evaluation of a bounding theorem due to Martin,[1] which provides an upper bound on the displacement rate at any point on the surface of a body in a state of steady creep. Also considered is a similar result by Palmer,[2] which provides a lower bound on the surface displacement rate.

In the past few years, various authors[3-5] have developed several deformation and work bounds. For structures under constant load, these bounds include effects of elastic and perfectly plastic material behavior in addition to creep deformation. A recent paper by Ponter[6] extends these results to structures in a state of creep subject to variable load. Such results will not be reviewed here, but it is notable that some of the difficulties associated with practical application of the bounding theorem to steady-creep behavior also exist in similar applications of bounding theorems to more complicated material response.

The bounding results due to Martin and Palmer for the steady-creep case are reviewed in Sec. II, where the restriction to n-power stress-strain rate relations is discussed. In Sec. III, these theorems are applied to several problems for which exact solutions are available, and the accuracy of the bounds for various equilibrated stress fields is established. A procedure for calculating displacement-rate bounds for complex structures using the finite-element method and the equilibrated elastic stress distribution is described in Sec. IV, together with an example. The results and their implication are summarized in Sec. V, where particular emphasis is placed on the potential value and general utility of bounding methods as a design tool.

II. DISPLACEMENT-RATE BOUNDING THEOREMS FOR STEADY-STATE CREEP

Under conditions of uniaxial stress, the most commonly accepted stress-strain-rate relationship for steady-state creep has the form

$$\dot{\epsilon}/\dot{\epsilon}_0 = (\sigma/\sigma_0)^n, \tag{1}$$

where σ denotes the uniaxial stress, $\dot{\epsilon}$ is the uniaxial creep strain rate, σ_0 and n are material constants, and $\dot{\epsilon}_0$ is the strain rate due to the stress σ_0. The generalization of Eq. 1 for multiaxial states of stress may be written as

$$\dot{\epsilon}_{ij}/\dot{\epsilon}_0 = \tfrac{3}{2}(\sigma_e/\sigma_0)^{n-1} s_{ij}/\sigma_0, \tag{2}$$

where

$$s_{ij} = \sigma_{ij} - \tfrac{1}{3}\sigma_{kk}\delta_{ij} \tag{3}$$

is the stress deviator, and σ_e denotes the effective stress defined as

$$\sigma_e^2 = \tfrac{3}{2} s_{ij} s_{ij}. \tag{4}$$

Although specific attention in this report is given to steady-state-creep behavior defined by Eq. 2, the bounding theorems to be considered are applicable to a large class of materials whose constitutive equations have the form

$$\dot{\epsilon}_{ij}/\dot{\epsilon}_0 = \varphi^n \frac{\partial\varphi}{\partial(\sigma_{ij}/\sigma_0)}, \tag{5}$$

where φ is homogeneous of degree one,* and φ^{n+1} is a convex function** of its argument. The necessity for restricting the class of material response to that defined by Eq. 5 is discussed later in this section. With $\varphi = \sigma_e/\sigma_0$, Eq. 2 is recovered and, since σ_e satisfies the conditions of homogeneity and convexity, the bounding theorems are applicable to materials characterized by Eq. 2.

The upper- and lower-bound displacement-rate theorems are based on an inequality derived by Martin[7] for materials having constitutive equations

---

*$\varphi(\sigma_{ij}/\sigma_0)$ is homogeneous of degree one, provided that $\varphi(\lambda\sigma_{ij}/\sigma_0) = \lambda\varphi(\sigma_{ij}/\sigma_0)$ for all positive values of λ. In addition, if φ is homogeneous of degree one, the following identity is satisifed: $(\sigma_{ij}/\sigma_0)\,\partial\varphi/[\partial(\sigma_{ij}/\sigma_0)] = \varphi$.

**$\varphi(\sigma_{ij}/\sigma_0)$ is a convex function if for any two arguments $\tilde{\sigma}_{ij}$ and $\hat{\sigma}_{ij}$, and any $0 \le \lambda \le 1$, $\varphi[\lambda(\tilde{\sigma}_{ij}/\sigma_0) + (1-\lambda)\,\hat{\sigma}_{ij}/\sigma_0] \le \lambda\varphi(\tilde{\sigma}_{ij}/\sigma_0) + (1-\lambda)\,\varphi(\hat{\sigma}_{ij}/\sigma_0)$.

of the form given by Eq. 5. This inequality states that, for a given body B of volume V and surface area A, in the absence of body forces,

$$\int_V \Omega(\sigma_{ij}^s)\, dV + \int_V W(\dot{\epsilon}_{ij}^c)\, dV \geq \int_A t_i^s \dot{u}_i^c\, dA, \tag{6}$$

where

$$W(\dot{\epsilon}_{ij}^c) = \int_0^{\dot{\epsilon}_{ij}^c} \sigma_{ij}\, d\dot{\epsilon}_{ij} \tag{7}$$

is the work function, and

$$\Omega(\sigma_{ij}^s) = \int_0^{\sigma_{ij}^s} \dot{\epsilon}_{ij}\, d\sigma_{ij} \tag{8}$$

is the complementary work function; σ_{ij}^s and t_i^s represent an arbitrary equilibrated set of stresses and surface tractions, and $\dot{\epsilon}_{ij}^c$, $\dot{u}_i^c$ represent an arbitrary compatible set of strain rates and velocities. Equation 6 can be shown to follow directly from Drucker's material stability postulate[8] or, alternatively, from the assumed convexity of the work function,[11] together with the principle of virtual work.

For a material characterized by Eq. 5, simple relationships exist between the rate of energy dissipation per unit volume,

$$\dot{D} = \dot{\epsilon}_{ij}\sigma_{ij}, \tag{9}$$

and the work and complementary work functions $W(\dot{\epsilon}_{ij})$ and $\Omega(\sigma_{ij})$, respectively. Using Eq. 5 and the restrictions on φ, Eqs. 7 and 8 become

$$W(\dot{\epsilon}_{ij}^c) = \frac{1}{n+1}\, \dot{\epsilon}_{ij}^c \sigma_{ij}^c, \tag{10}$$

and

$$\Omega(\sigma_{ij}^s) = \frac{n}{n+1}\, \dot{\epsilon}_{ij}^s \sigma_{ij}^s. \tag{11}$$

The term σ_{ij}^c in Eq. 10 is related to $\dot{\epsilon}_{ij}^c$ through Eq. 5 and need not meet any equilibrium requirements. Similarly, $\dot{\epsilon}_{ij}^s$ in Eq. 11 is related to σ_{ij}^s through Eq. 5 and need not satisfy the compatibility conditions. With the aid of Eqs. 10 and 11, inequality 6 becomes

$$\frac{1}{n+1} \int_V \sigma_{ij}^s \dot{\epsilon}_{ij}^s\, dV + \frac{n}{n+1} \int_V \sigma_{ij}^c \dot{\epsilon}_{ij}^c\, dV \geq \int_A t_i^s \dot{u}_i^c\, dA. \tag{12}$$

A standard boundary-value problem is considered, for which surface tractions t_i are prescribed on a part of the boundary A_t, with zero velocity prescribed on the remainder of the boundary $A_u = A - A_t$. The body-force density is taken to be zero, and material behavior is assumed to be defined by the stress-strain-rate relationships of Eq. 5, for some admissible function φ; σ_{ij}, $\dot{\epsilon}_{ij}$, and $\dot{u}_i$ are used to denote the actual solution for this problem.

Since $\dot{\epsilon}_{ij}$ and $\dot{u}_i$ are a compatible set of strain rates and velocities, they may be used in Eq. 12 to obtain

$$\frac{1}{n+1}\int_V \sigma_{ij}^s \dot{\epsilon}_{ij}^s \, dV + \frac{n}{n+1}\int_V \sigma_{ij}\dot{\epsilon}_{ij} \, dV \geq \int_A t_i^s \dot{u}_i \, dA. \tag{13}$$

Equating internal and external energy-dissipation rates,

$$\int_V \sigma_{ij}\dot{\epsilon}_{ij} \, dV = \int_A t_i \dot{u}_i \, dA, \tag{14}$$

Eq. 13 becomes

$$\int_A \left(t_i^s - \frac{n}{n+1} t_i\right) \dot{u}_i \, dA \leq \frac{1}{n+1}\int_V \sigma_{ij}^s \dot{\epsilon}_{ij}^s \, dV. \tag{15}$$

Inequality 15 can now be used to obtain an upper bound on the displacement rate at an arbitrary point Q on the surface A_t by choosing t_i^s on A_t equal to $[n/(n+1)]t_i$ plus a concentrated load of arbitrary magnitude at Q. Let P_i denote the added load and $(\dot{u}_Q)_i$ the displacement rate components at Q. For this choice of t_i^s,

$$P_i(\dot{u}_Q)_i \leq \frac{1}{n+1}\int_V \sigma_{ij}^s \dot{\epsilon}_{ij}^s \, dV. \tag{16}$$

An upper bound on $(\dot{u}_Q)_i$ is thus determined in terms of an arbitrary equilibrated stress field associated with surface tractions $[n/(n+1)]t_i$ plus the added load P_i.

Finally, with the use of Eq. 2, we may write Eq. 16 for a particular velocity component as

$$\dot{u}_Q \leq \frac{1}{P}\frac{1}{n+1}\frac{\dot{\epsilon}_0}{\sigma_0^n}\int_V (\sigma_e^s)^{n+1} \, dV, \tag{17}$$

where σ_e^s denotes the effective stress associated with the equilibrated stresses σ_{ij}^s. It should be remembered that the stress field σ_{ij}^s is a function of the arbitrary concentrated load P. In practical applications, an admissible stress field σ_{ij}^s is chosen and that value of P is determined that minimizes the right-hand side of Eq. 17. The bound so obtained represents the least upper bound associated with the chosen equilibrated field σ_{ij}^s.

Following Palmer,[2] the lower-bound theorem is developed by replacing the equilibrium set σ_{ij}^s, t_i^s with the solution set σ_{ij}, t_i in inequality 12, and using Eq. 14 to obtain

$$\frac{1}{n+1}\int_A t_i \dot{u}_i \, dA + \frac{n}{n+1}\int_V \sigma_{ij}^c \dot{\epsilon}_{ij}^c \, dV \geq \int_A t_i \dot{u}_i^c \, dA. \tag{18}$$

Multiplying inequality 18 by a positive constant β and adding inequality 15, we obtain, after rearrangement,

$$\int_A \left(\frac{\beta+n}{n+1} t_i - t_i^s\right) \dot{u}_i \, dA \geq \beta\left(\int_A t_i \dot{u}_i^c \, dA - \frac{n}{n+1}\int_V \sigma_{ij}^c \dot{\epsilon}_{ij}^c \, dV\right) - \frac{1}{n+1}\int_V \sigma_{ij}^s \dot{\epsilon}_{ij}^s \, dV. \tag{19}$$

Let $\dot{u}_Q$ denote, as before, the displacement rate at the surface point Q. If t_i^s is taken equal to $[(\beta+n)/(n+1)]t_i$ on A_t plus a concentrated load P at Q in a direction opposite to $\dot{u}_Q$, inequality 19 becomes

$$\dot{u}_Q \geq \frac{1}{P}\left[\beta\left(\int_A t_i \dot{u}_i^c \, dA - \frac{n}{n+1}\int_V \sigma_{ij}^c \dot{\epsilon}_{ij}^c \, dV\right) - \frac{1}{n+1}\int_V \sigma_{ij}^s \dot{\epsilon}_{ij}^s \, dV\right]. \tag{20}$$

The computation of a lower bound requires the selection of an admissible velocity field $\dot{u}_i^c$ in addition to the choice for an equilibrated stress field σ_{ij}^s. Once $\dot{u}_i^c$ and σ_{ij}^s are chosen, the constants β and P are determined so as to maximize the right-hand side of inequality 20. The lower bound determined through this procedure represents the greatest lower bound associated with the particular fields $\dot{u}_i^c$ and σ_{ij}^s.

Inequalities 17 and 20 provide a means for bounding the displacement rate at a point on the surface of a structure in the process of steady creep. The accuracy and sensitivity of these bounds to the assumed form of the velocity and stress fields required in inequalities 17 and 20 are considered in Sec. III.

The restriction of the bounding theorems to materials whose stress-strain-rate relations have the form given in Eq. 5 is to ensure that the work function $W(\dot{\epsilon}_{ij})$, or the complementary work function $\Omega(\sigma_{ij})$, is a constant

multiple of the rate of energy dissipation per unit volume, as given by Eqs. 10 and 11. In the upper-bound theorem, for example, the volume integral appearing in inequality 6

$$\int_V W(\dot{\epsilon}_{ij}^c)\, dV = \int_V \lambda \sigma_{ij}^c \dot{\epsilon}_{ij}^c\, dV, \tag{21}$$

where $\lambda = n/(n+1)$, can be calculated in terms of surface data through the principle of virtual work, since λ is a constant. If λ is not constant, the reduction of $\int_V W(\dot{\epsilon}_{ij}^c)\, dV$ to a surface integral is generally not obvious.

To illustrate this point, we consider the steady-state creep of a material whose stress-strain-rate relationship for uniaxial tension is given by

$$\dot{\epsilon} = A \exp(\sigma/\sigma_0), \tag{22}$$

where A and σ_0 are material constants.* A suitable generalization of Eq. 22 to three-dimensional states of stress is given by

$$\dot{\epsilon}_{ij} = \frac{3}{2} \frac{A[\exp(\sigma_e/\sigma_0)]}{\sigma_e} s_{ij}. \tag{23}$$

Using Eqs. 7 and 8, together with Eq. 23 yields

$$\Omega(\sigma_{ij}) = \frac{\sigma_0}{\sigma_e} \dot{D} - A\sigma_0, \tag{24}$$

and

$$W(\dot{\epsilon}_{ij}) = (1 - \sigma_0/\sigma_e)\, \dot{D} + A\sigma_0, \tag{25}$$

where

$$\dot{D} = \sigma_{ij}\dot{\epsilon}_{ij} = A\sigma_e \exp(\sigma_e/\sigma_0). \tag{26}$$

Equations 24 and 25 imply that inequality 6 may be expressed as

$$\int_V \frac{\sigma_0}{\sigma_e^s} \dot{D}^s\, dV + \int_V (1 - \sigma_0/\sigma_e^c)\, \dot{D}^c\, dV \geq \int_S t_i^s \dot{u}_i^c\, dS. \tag{27}$$

*The results obtained using this form are typical of results obtained when the constitutive equation involves combinations of hyperbolic functions.

There appears to be no simple representation in terms of surface integrals for either volume integral on the left-hand side of inequality 27; hence the utility of this expression is not apparent.

It is interesting to note that, for a one-dimensional stress-strain-rate relationship of the form

$$\dot{\epsilon}/\dot{\epsilon}_0 = f(\sigma/\sigma_0), \tag{28}$$

where f is arbitrary, the condition that the complementary work function be a constant multiple of the energy-dissipation-rate density, i.e.,

$$\Omega(c) = c\dot{D} \tag{29}$$

where c is constant, implies that

$$f = \dot{\sigma}/\sigma_0^{\frac{1-c}{c}}, \tag{30}$$

which is the one-dimensional power law.

The general solution of the integral equation equivalent to Eq. 29 for three-dimensional states of stress is not immediate; however, a class of solutions is given by

$$\dot{\epsilon}_{ij}/\dot{\epsilon}_0 = f(\sigma_{ij}/\sigma_0) = \frac{1}{n+1} \frac{\partial \varphi^{n+1}}{\partial\left(\frac{\sigma_{ij}}{\sigma_0}\right)}, \tag{31}$$

provided that φ is homogeneous of degree one in the variables σ_{ij}/σ_0. This solution is equivalent to restricting the stress-strain-rate relations to the form of Eq. 5.

The limitation of practical bounding theorems to creep laws of the power-law type is not necessarily a serious disadvantage, since creep representations such as the exponential law given by Eq. 22 can be, in many instances, adequately approximated by the power-law relationship of Eq. 1 over a given stress range.

III. APPLICATIONS OF THE BOUNDING THEOREMS

A. Analytical Optimization

The steady-state creep-displacement-rate bounding theorems described in Sec. II have been applied to several problems for which exact, closed-form solutions are available. These examples give an indication of the accuracy of the bounds for various structures and the sensitivity of the bounds to assumed forms of the required equilibrated stress and compatible strain rate and velocity fields.

For reasons discussed near the end of Sec. III.C below, much of the work presented here concerns the determination of upper bounds on the surface-displacement rate. In most practical applications of the upper-bound theorem, the quantity on the right-hand side of inequality 17 cannot be conveniently optimized analytically; therefore, numerical minimization will be necessary.

One type of problem for which the optimum value of the added load P can be determined in closed form is that of a structure subjected to a concentrated load R at a point Q on the surface. An upper bound on the displacement rate at point Q in the direction of the load R is sought, and, from inequality 17,

$$\dot{u}_Q \le \frac{1}{P}\frac{1}{n+1}\frac{\dot{\epsilon}_0}{\sigma_0^n}\int_V (\sigma_e^s)^{n+1}(\sigma_{ij}^s/\sigma_0)\,dV, \tag{32}$$

where σ_{ij}^s is an arbitrary stress field in equilibrium with a surface load $\lambda = [n/(n+1)]R + P$. Writing

$$\sigma_{ij}^s = \lambda\hat{\sigma}_{ij}, \tag{33}$$

where $\hat{\sigma}_{ij}$ is any equilibrated stress distribution due to a unit load at point Q in the direction of R, and recalling the definition of effective stress in Eq. 4, Eq. 32 may be written as

$$\dot{u}_Q \le \frac{\dot{\epsilon}_0}{\sigma_0^n}R^n\frac{1}{n+1}\left(\frac{n}{n+1}\right)^{n+1}\frac{\left(1+\frac{n+1}{n}P/R\right)^{n+1}}{P/R}\int_V (\sigma_e^s)^{n+1}(\hat{\sigma}_{ij}/\sigma_0)\,dV. \tag{34}$$

From inequality 34, the optimum value of P/R is

$$P/R = \frac{1}{n+1}; \tag{35}$$

therefore, the least upper bound for a given stress distribution $\hat{\sigma}_{ij}$ is

$$\dot{u}_Q \le \frac{\dot{\epsilon}_0}{\sigma_0^n} R^n \int_V (\sigma_e^s)^{n+1} (\hat{\sigma}_{ij}/\sigma_0)\, dV. \tag{36}$$

The results given by Eq. 35 and inequality 36 can be shown to be valid for certain other structure loading cases; however, for most problems of practical interest, the optimum value of the added load P must be determined numerically.

B. Cantilever Beam

Consider a cantilever beam subjected to a concentrated load R at the free end $x = \ell$, as shown in Fig. 1. The beam is in a state of steady creep defined by the stress-strain-rate relation*

$$\dot{\epsilon}/\dot{\epsilon}_0 = |\sigma/\sigma_0|^n \operatorname{sgn} \sigma, \tag{37}$$

where

$$\operatorname{sgn} \sigma \equiv \begin{cases} 1 & \text{if } \sigma > 0 \\ 0 & \text{if } \sigma = 0 \\ -1 & \text{if } \sigma < 0. \end{cases} \tag{38}$$

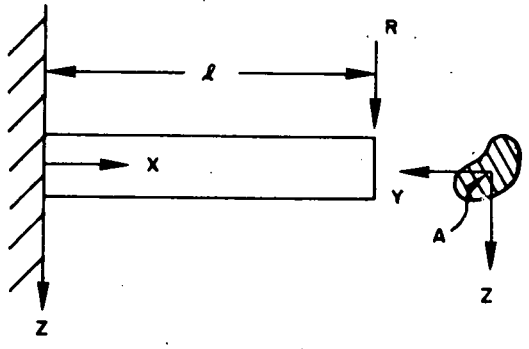

Fig. 1
Cantilever Beam with Concentrated Load at Free End

Suppose that bounds are required on the rate of deflection $\dot{\delta}$ at the free end. With the usual kinematic assumptions for beam theory, the bending stress is given by

$$\sigma = \frac{M}{I_n} |z|^{1/n} \operatorname{sgn} z, \tag{39}$$

and the rate of deflection is

$$\dot{w} = \frac{\dot{\epsilon}_0 R^n}{\sigma_0^n I_n^n (n+1)(n+2)} [(\ell - x)^{n+2} + (n+2)\, \ell^{n+1} x - \ell^{n+2}], \tag{40}$$

*Equation 37 is a simple modification of Eq. 1, valid for arbitrary values of the creep exponent n.

where M denotes the bending moment, and

$$I_n \equiv \int_A |z|^{(1/n)+1}\, dA \tag{41}$$

is a constant determined by the shape of the beam cross section. Thus the actual rate of deflection at $x = \ell$ is given by

$$\dot{\delta} = \frac{\dot{\epsilon}_0 R^n \ell^{n+2}}{\sigma_0^n I_n^n (n+2)}. \tag{42}$$

An upper bound on $\dot{\delta}$ may be obtained from inequality 15 which, for this problem, can be expressed as

$$\dot{\delta} \le \frac{\dot{\epsilon}_0}{\sigma_0^n (n+1)} \left(P^{-1} \int_V |\sigma^s|^{n+1}\, dV \right), \tag{43}$$

where σ^s represents any equilibrated bending-stress distribution due to a concentrated load $[n/(n+1)]R + P$ at $x = \ell$. From the discussion in Sec. III.A, the "best" upper bound for a given choice of σ^s occurs when $P = R/(n+1)$. Choosing σ^s to be the elastic bending stress

$$\sigma^s = \frac{M}{I_1} |z| \operatorname{sgn} z, \tag{44}$$

the least upper bound based on Eq. 44 is obtained from inequality 43 as

$$\dot{\delta} \le \frac{\dot{\epsilon}_0 R^n \ell^{n+2}}{\sigma_0^n I_n^n (n+2)} \frac{I_n^n \int_A |z|^{n+1}\, dA}{I^{n+1}}; \tag{45}$$

and by comparison with Eq. 42, the ratio of the least upper bound based on elastic stresses to the actual value of the displacement rate at $x = \ell$, is given by

$$E_n^+ = \frac{I_n^n \int_A |z|^{n+1}\, dA}{I^{n+1}} \tag{46}$$

and depends, in general, on the cross-sectional shape and creep exponent n.

For a beam with rectangular cross section, Eq. 46 implies

$$E_n^+ = \frac{3}{n+2} \left(\frac{3n}{2n+1} \right)^n \tag{47}$$

and is independent of the section dimensions.

We next consider a class of equilibrated bending-stress distributions σ^s given by

$$\sigma^s = \frac{M}{I_m} |z|^{1/m} \operatorname{sgn} z, \tag{48}$$

defined by the parameter m. For m = 1, this reduces to the elastic stress state, for m = n it gives the actual stress state, and, as $m \to \infty$, it reduces to the plastic stress state. Using Eq. 48 in inequality 43, the ratio of the least upper bound for a given value of m in Eq. 48 to the actual displacement rate is determined as

$$R^+_{m,n} = \frac{I_n^n}{I_m^{n+1}} \int_A |z|^{(n+1)/m} \, dA. \tag{49}$$

Clearly $R^+_{1,n} = E^+_n$, and we define

$$P^+_n = \lim_{m \to \infty} R^+_{m,n} \tag{50}$$

to denote the ratio of the least upper bound based on the plastic stress state to the actual displacement rate.*

For the particular case of a rectangular cross section, Eq. 49 is evaluated as

$$R^+_{m,n} = \left(\frac{2 + 1/m}{2 + 1/n}\right)^n \left(\frac{2 + 1/m}{1 + (n+1)/m}\right) \tag{51}$$

and, as with the case for m = 1., is independent of the cross-section dimensions.

Upper-bound data for the rectangular cross section are shown in Figs. 2 and 3 as a function of the creep exponent n. For this and other examples considered in Sec. III, bounding data are presented for a range of creep exponent ($1 \le n \le 10$) and are therefore appropriate for most structural metals of interest.

Upper-bound data based on the elastic stress state shown in Fig. 2 indicate a deterioration of accuracy for increasing values of n, with severe loss of accuracy for values of $n > 10$.

The degree of accuracy required for an upper or lower bound depends to a large extent on the design problem to which the bounding theorem is applied. As an example, from Fig. 2, for a value of the creep exponent n = 5,

*The definitions of $R^+_{m,n}$, E^+_n, and P^+_n are used consistently throughout Sec. III and represent a measure of the upper-bound accuracy based on a specific choice for the equilibrated stress field σ^s_{ij}.

the upper bound is approximately twice the actual displacement rate $\dot{\delta}$. If the design allowable displacement rate is larger than the upper bound determined from Fig. 2, the accuracy of the upper bound is sufficient and indeed immaterial.

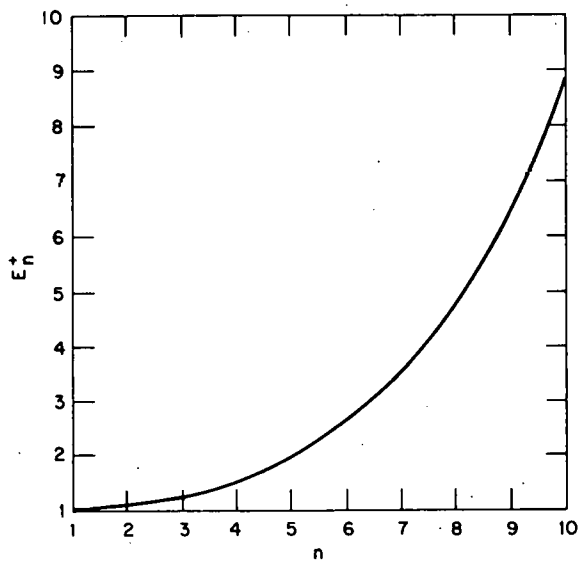

Fig. 2. Least-upper-bound Data for Cantilever-beam Example Based on Elastic Stresses: Variation of E_n^+ with Creep Exponent n for a Beam with Rectangular Cross Section

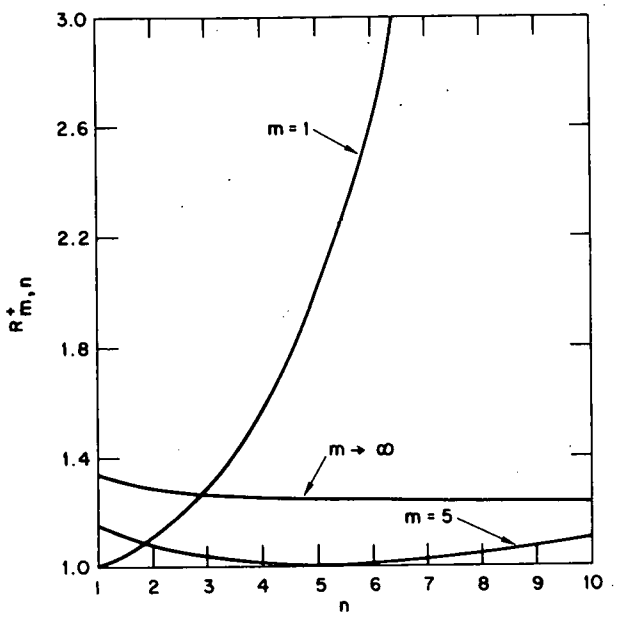

Fig. 3. Least-upper-bound Data for Cantilever-beam Example Based on a Class of Equilibrated Stress Distributions: Variation of $R_{m,n}^+$ with Creep Exponent n for a Beam with Rectangular Cross Section

With increased effort, the accuracy of the bounds can be improved by "better" choices of the field variables σ_{ij}^s and $\dot{u}_i^c$; therefore, at some point, a trade-off between bound accuracy and computer cost must be established.

The variation of $R_{m,n}^+$ with creep exponent n as given by Eq. 51 is shown in Fig. 3 for values of m = 1 and 5, and the limiting case $m \to \infty$. A direct comparison between upper bounds based on the elastic stress state (m = 1) and plastic stress state ($m \to \infty$) is presented, and the superior accuracy of the bound based on the plastic stress state for $n \geq 3$ is apparent. Furthermore, the bound based on the plastic stress state is approximately constant over the range $1 \leq n \leq 10$, while the bound based on the elastic stress state varies rapidly for small changes in creep exponent n. This behavior must be kept in mind when applying the bounding theorems to structures where the experimentally determined value of the creep exponent n may be subject to a large degree of uncertainty.

The upper-bound curve for m = 5, in Fig. 3, is representative of results obtained for other finite values of $m > 1$. The "flatness" of this curve near n = 5 is encouraging and suggests that quite accurate upper bounds are possible when the equilibrated stress field σ_{ij}^s is "near" the actual stress state.

A lower bound on $\dot{\delta}$ is now developed through use of inequality 20 and the particular choice of a consistent* velocity field $\dot{w}^c$, given by

$$\dot{w}^c = \alpha[(\ell - x)^3 + 3\ell^2 x - \ell^3], \tag{52}$$

where α is a constant. Equation 52 is appropriate for the linear case $n = 1$ and can be obtained from the elastic solution by simply replacing displacements with displacement rates.

Using Eq. 52, the quantity

$$Q \equiv \int_A t_i \dot{u}_i^c \, dA - \frac{n}{n+1} \int_V \sigma_{ij}^c \dot{\epsilon}_{ij}^c \, dV \tag{53}$$

in inequality 20 can be expressed as

$$Q = 2\alpha R \ell^3 - \frac{n}{n+1} \frac{n}{2n+1} \frac{\sigma_0 I_n}{\dot{\epsilon}_0^{1/n}} (6\alpha)^{1+(1/n)} \ell^{2+(1/n)}, \tag{54}$$

and the value

$$\alpha = \left(\frac{2R}{\sigma_0 I_n}\right)^n \frac{\dot{\epsilon}_0 \ell^{n-1}}{6^{n+1}\left(\frac{n}{1+2n}\right)^n} \tag{55}$$

is selected to give

$$Q_{max} = \frac{\frac{1}{n+1}\left(\frac{1+2n}{n}\right)^n \left(\frac{1}{3}\right)^{n+1} (R^{n+1} \ell^{n+2} \dot{\epsilon}_0)}{(\sigma_0 I_n)^n}. \tag{56}$$

The equilibrated stress field is chosen as the elastic bending stress given by Eq. 44, due to a concentrated load $[R(\beta + n)/(n + 1) - P]$ at $x = \ell$, and the inequality 20 with the aid of Eq. 56 may be expressed as

$$\dot{\delta} \geq \frac{\dot{\epsilon}_0 R^n \ell^{n+2}}{\sigma_0^n I_n^n (n+2)} \left[\frac{1}{n+1} I(\beta, P/R)\right], \tag{57}$$

where

$$I(\beta, P/R) \equiv (P/R)^{-1} \left[a\beta - b\left(\frac{\beta + n}{n+1} - P/R\right)^{n+1}\right], \tag{58}$$

*A consistent or admissible velocity field is used here to denote any continuous velocity distribution that satisfies the prescribed velocity boundary conditions.

with

$$\left.\begin{aligned} a &= (n+2)\left(\frac{1+2n}{n}\right)^n\left(\frac{1}{3}\right)^{n+1}, \\ \text{and} \\ b &= \frac{I_n^n}{I^{n+1}}\int_A |z|^{n+1}\, dA. \end{aligned}\right\} \tag{59}$$

For a given value of P/R, it may be shown that $I(\beta, P/R)$ has a maximum value along the line

$$\beta = (n+1)[(a/b)^{1/n} + P/R] - n \tag{60}$$

as $P/R \to \infty$. The maximum value of I obtained is

$$I_{max} = (n+1)\, a; \tag{61}$$

therefore, the ratio of the greatest lower bound based on the elastic state to the actual displacement rate $\dot{\delta}$ is given by

$$\bar{E}_n = a. \tag{62}$$

We note that Eq. 62 is valid for all beam cross sections, which is due to the fact that, for this problem, the greatest lower bound is independent of the assumed equilibrated stress field and depends solely on the choice of the velocity $\dot{w}^c$.

Using a similar procedure, the ratio of the greatest lower bound, based on a class of velocity fields

$$\dot{w}^c = \alpha[(\ell - x)^{m+2} + (m+2)\,\ell^{m+1}x - \ell^{m+2}], \tag{63}$$

defined by the constants α and m, to the actual displacement rate is determined as

$$\bar{R}_{m,n} = \frac{n+2}{m+2}\left[\frac{m+n(1+m)}{n(m+2)}\right]^n, \tag{64}$$

independent of the cross-section shape. The variation of $\bar{R}_{m,n}$ with creep exponent n is shown in Fig. 4 for several values of the parameter m. For the elastic case ($m = 1$) and a creep exponent $n = 5$, the lower bound is approximately one-half the actual displacement rate. The lower bound based on other values of m in the range $1 \le m \le 10$ is significantly more accurate.

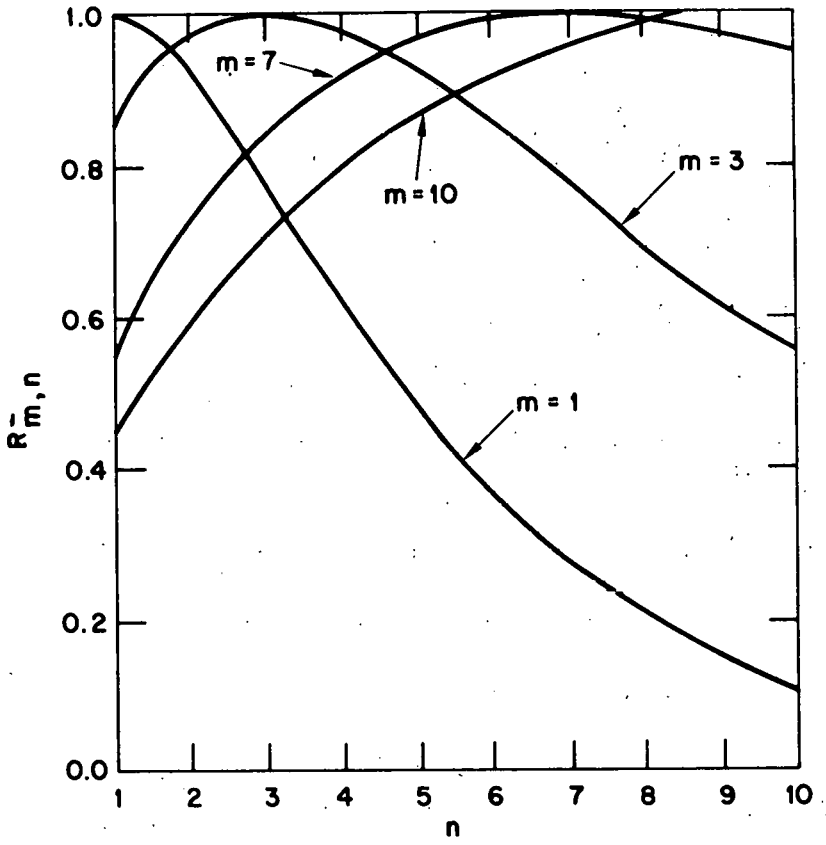

Fig. 4. Greatest-lower-bound Data for Cantilever-beam Example Based on a Class of Consistent Velocity Fields: Variation of $\bar{R}_{m,n}$ with Creep Exponent n for a Beam of Arbitrary Cross Section

Again, the "flatness" of the curves in the vicinity of m = n suggests that sharp lower bounds can be obtained for velocity fields that are "near" the actual velocity field.

C. Pressurized Cylindrical Tube

Consider a long cylindrical tube as shown in Fig. 5, subjected to constant internal and external pressure, p_i and p_o, at the inner and outer lateral surfaces $r = r_i$ and $r = r_o$, respectively, with the plane ends constrained by smooth rigid plates. Denoting the displacement components relative to the (r,θ,z) cylindrical coordinate system by (u,v,w), symmetry and the assumption of a state of generalized plane strain lead to

$$\left.\begin{aligned} &u = u(r) \\ &\text{and} \\ &v = w = 0 \end{aligned}\right\}. \tag{65}$$

The nonzero components of strain are given by

$$\left.\begin{aligned} &\epsilon_{rr} = \frac{du}{dr} \\ &\text{and} \\ &\epsilon_{\theta\theta} = u/r \end{aligned}\right\}, \tag{66}$$

and equilibrium requires

$$\frac{d\sigma_{rr}}{dr} + \frac{\sigma_{rr} - \sigma_{\theta\theta}}{r} = 0 \tag{67}$$

together with the boundary conditions

$$\left.\begin{aligned} &\sigma_{rr} = -p_i, \quad r = r_i, \\ &\text{and} \\ &\sigma_{rr} = -p_o, \quad r = r_o. \end{aligned}\right\} \tag{68}$$

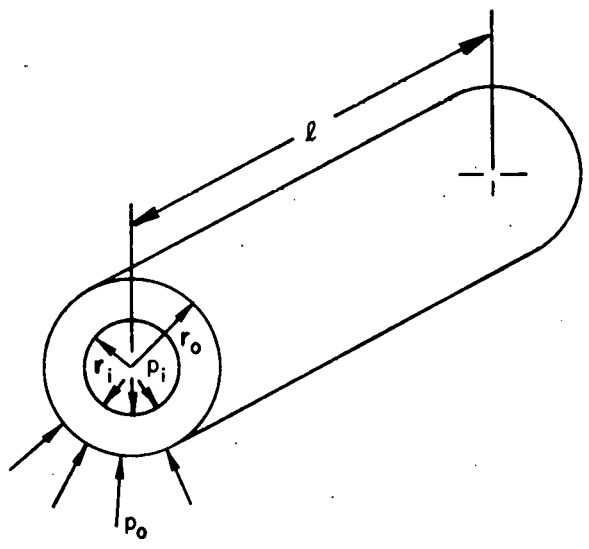

Fig. 5
Pressurized Long, Circular Cylinder

In addition, the tube is assumed to be incompressible, so that

$$\frac{du}{dr} + u/r = 0. \tag{69}$$

The solution for an elastic material is given below for reference:

$$\left.\begin{aligned} \sigma_{rr} &= -\frac{A}{r^2} + B, \\ \sigma_{\theta\theta} &= \frac{A}{r^2} + B, \\ \sigma_{zz} &= A, \end{aligned}\right\} \tag{70}$$

and

$$u = C/r,$$

where

$$\left.\begin{aligned} A &= (p_o - p_i)\frac{r_i^2 r_o^2}{r_i^2 - r_o^2}, \\ B &= -p_i + (p_o - p_i)\frac{r_o^2}{r_i^2 - r_o^2}, \\ C &= \frac{3A}{2E}, \end{aligned}\right\} \tag{71}$$

and E is Young's modulus.

The solution for steady-state creep based on the stress-strain-rate relations of Eq. 2 can be written as

$$\left.\begin{aligned} \sigma_{rr} &= Ar^{-2/n} + B, \\ \sigma_{\theta\theta} &= A\left(1 - \frac{2}{n}\right) r^{-2/n} + B, \\ \sigma_{zz} &= A\left(1 - \frac{1}{n}\right) r^{-2/n} + B, \end{aligned}\right\} \tag{72}$$

and

$$\dot{u} = C/r,$$

where $\dot{u}$ denotes the radial velocity and

$$A = \frac{p_o - p_i}{r_i^{-2/n} - r_o^{-2/n}},$$

$$B = -p_i - \frac{(p_o - p_i)\, r_i^{-2/n}}{r_i^{-2/n} - r_o^{-2/n}},$$

and

$$C = \frac{\dot{\epsilon}_0 \left(\sqrt{3}\right)^{n+1}}{2} (\sigma_0 n)^{-n} \left(\frac{p_i - p_o}{r_i^{-2/n} - r_o^{-2/n}} \right)^n . \qquad (73)$$

We assume that an upper bound on the velocity of the inner surface, $r = r_i$, is required; therefore, inequality 15 is applied to the case for which tractions t_i^s are given by

$$t_i^s = \frac{n}{n+1} t_i + p^*, \quad r = r_i,$$

and

$$t_i^s = \frac{n}{n+1} t_i, \qquad r = r_o, \qquad (74)$$

where p^* represents an arbitrary additive pressure. On the plane ends of the cylinder, t_i^s is allowed to assume any value in order to satisfy equilibrium. Accordingly, inequality 15 becomes

$$(2\pi r_i \ell) p^* \dot{u}\big|_{r=r_i} \le \frac{\dot{\epsilon}_0}{\sigma_0^n (n+1)} \int_V (\sigma_e^s)^{n+1} \, dV, \qquad (75)$$

where the effective stress for this problem is given by

$$\sigma_e^s = \frac{\sqrt{3}}{2} \left(\sigma_{\theta\theta}^s - \sigma_{rr}^s \right). \qquad (76)$$

Using Eq. 76 together with the equilibrium Eq. 67, inequality 75 may be rewritten as

$$\dot{u}\big|_{r=r_i} \le \frac{\dot{\epsilon}_0}{r_i (n+1)\, \sigma_0^n} \left(\frac{\sqrt{3}}{2} \right)^{n+1} \frac{1}{p^*} \int_{r_i}^{r_o} \left(r \frac{d\sigma_{rr}^s}{dr} \right)^{n+1} r \, dr. \qquad (77)$$

Since equilibrium is satisfied, the only restriction on σ^s_{rr} is that it satisfy the boundary conditions

$$\left.\begin{aligned} \sigma^s_{rr} &= -\frac{n}{n+1}\, p_i - p^*, \qquad r = r_i, \\ \text{and} \\ \sigma^s_{rr} &= -\frac{n}{n+1}\, p_o, \qquad r = r_o. \end{aligned}\right\} \tag{78}$$

Using the elastic radial stress distribution appropriate to Eqs. 78, given by Eqs. 70 with

$$A = \frac{n}{n+1}(p_o - p_i)\,\frac{r_i^2 r_o^2}{r_i^2 - r_o^2} - p^*\,\frac{r_i^2 r_o^2}{r_i^2 - r_o^2}, \tag{79}$$

and minimizing the right-hand side of inequality 77, the least upper bound based on elastic stresses is obtained as

$$\dot{u}\big|_{r=r_i} \le \left[\frac{1}{r_i}\,\frac{(\sqrt{3})^{n+1}}{2}\left(\frac{p_i - p_o}{\sigma_0 n}\right)^n \frac{r_i^2 r_o^2}{\left(r_o^{2/n} - r_i^{2/n}\right)^n}\right] E_n^+, \tag{80}$$

where

$$E_n^+ \equiv n^{n-1}\left[\frac{1 - (r_i/r_o)^{2n}}{1 - (r_i/r_o)^2}\right]\left[\frac{1 - (r_i/r_o)^{2/n}}{1 - (r_i/r_o)^2}\right]^n \tag{81}$$

is, by comparison of inequality 80 with Eqs. 72 and 73, the ratio of the least upper bound based on elastic stresses to the actual value of the radial velocity at $r = r_i$. For thin cylindrical shells of thickness t, Eq. 81 can be approximated by

$$E_n^+ = 1 + \frac{(n-1)^2(n+1)}{6n}(t/r_i)^2 + O(t/r_i)^3, \tag{82}$$

which indicates that, for a given value of the creep exponent n, the least upper bound rapidly approaches the actual velocity as $r_i/r_o \to 1$.

The class of radial stress distributions

$$\sigma^s_{rr} = A_m r^{-2/m} + B_m \tag{83}$$

that contains the elastic state for $m = 1$, the actual stress state for $m = n$, and the plastic stress state in the limit as $m \to \infty$, is considered. The constants A_m and B_m are determined from the boundary conditions of Eqs. 78.

Using Eq. 83 in inequality 77, the ratio of the least upper bound for a specific value of m to the actual velocity at the inner surface, $r = r_i$, is given by

$$R^+_{m,n} = \left(\frac{n}{m}\right)^n (m-n-1)^{-1} \left(\frac{r_i^{2/m} r_o^{2/m}}{r_o^{2/m} - r_i^{2/m}}\right)^{n+1} \left[r_o^{(2/m)(m-n-1)} - r_i^{(2/m)(m-n-1)}\right] \frac{\left(r_o^{2/n} - r_i^{2/n}\right)^n}{r_i^2 r_o^2}, \qquad (84)$$

and it may be shown that

$$R^+_{n,n} = 1,$$

$$R^+_{1,n} = E^+_n,$$

and

$$P^+_n \equiv \lim_{m\to\infty} R^+_{m,n} = \frac{-\frac{1}{2}\left[1 - (r_i/r_o)^2\right]}{(r_i/r_o)^2 \ln (r_i/r_o)} \left[\frac{-\frac{n}{2}\left[1 - (r_i/r_o)^{2/n}\right]}{\ln (r_i/r_o)}\right]^n. \qquad (85)$$

As before, P^+_n represents the ratio of the least upper bound based on the plastic stress state to the actual value of the velocity.

The variation of E^+_n with creep exponent n for a cylinder with $r_i/r_o = 0.5$ is shown in Fig. 6, and the variation of E^+_n as a function of r_i/r_o is shown in Fig. 7, for various values of n. These data indicate that the accuracy of

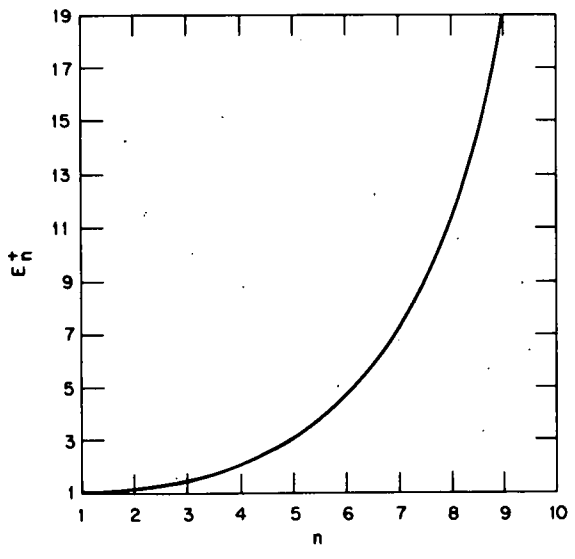

Fig. 6. Least-upper-bound Data for Pressurized Circular Tube Based on Elastic Stress Distribution: Variation of E^+_n with Creep Exponent n for a Tube with $r_i/r_o = 0.5$

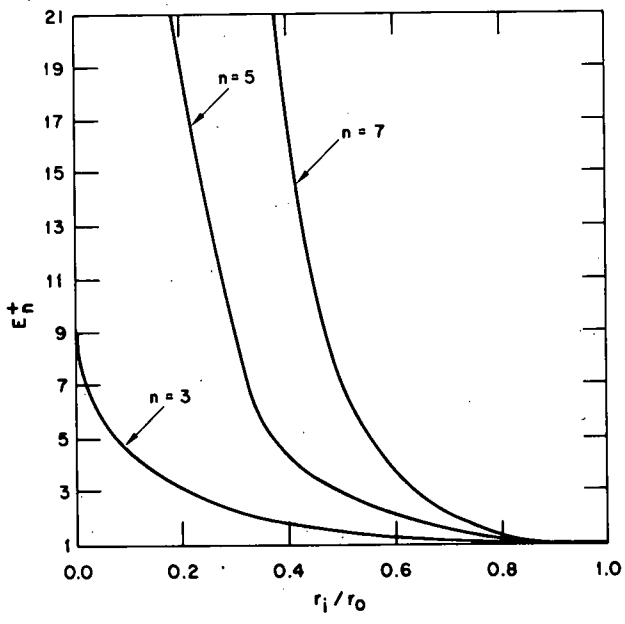

Fig. 7. Least-upper-bound Data for Pressurized Circular Tube Based on Elastic Stress Distribution: Variation of E^+_n with r_i/r_o for Several Values of Creep Exponent n

the upper bound deteriorates rapidly for large values of n. For n = 8, and for $r_i/r_o = 1/2$, the upper bound based on elastic stresses is approximately an order of magnitude greater than the actual velocity. Errors of this magnitude may be too severe for design purposes, and improvements are required.

The curves in Fig. 7 and Eq. 82 indicate that accurate bounds are obtained for relatively thin structures ($r_i/r_o > 0.7$), even for large values of the creep exponent n.

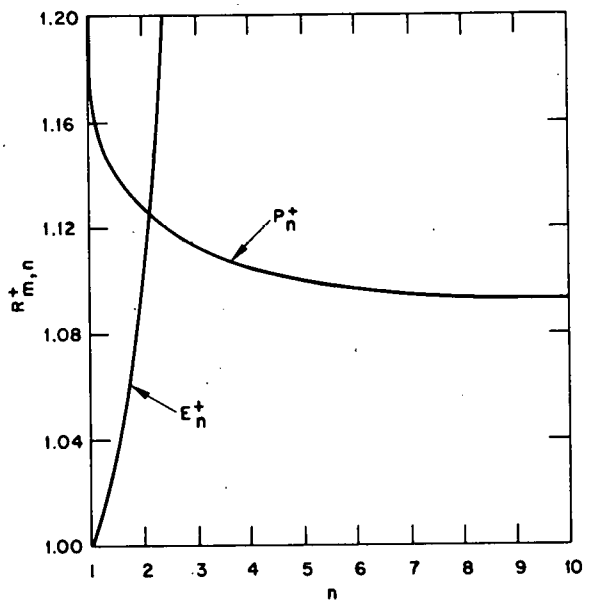

Fig. 8. Least-upper-bound Data for Pressurized Circular Tube Based on a Class of Equilibrated Stress Distributions: Variation of $R^+_{m,n}$ with Creep Exponent n for a Tube with $r_i/r_o = 0.5$

Figure 8 compares the least upper bounds based on the elastic and plastic stress states for a cylinder with $r_i/r_o = 1/2$. For values of the creep exponent n in the range of interest, bounds based on the plastic stress state are far superior to those based on the elastic stress state. For a material with creep exponent n = 8, the least upper bound based on the plastic stress state is about 10% larger than the actual value of the velocity and represents a useful bound from a design point of view. Unfortunately, at present, the cost involved in generating the plastic state of stress for a given structure at collapse is significantly greater than the cost for developing an elastic solution.

Application of the lower-bound theorem, in the form of inequality 20, to this problem leads to a determination of an exact lower bound on the radial velocity at the inner surface $r = r_i$. Any assumed velocity field $\dot{u}_i^c$ must be consistent with the incompressibility condition of Eq. 69 and therefore must be of the form

$$\dot{u}_i^c = C/r, \qquad (86)$$

which is the actual velocity field for the appropriate value of the constant C.

The pressurized tube and the other remaining problems considered in Sec. III are essentially kinematically determinant. Constraint equations on the velocity field, such as incompressibility, dictate the required functional form for the velocity; therefore, the use of arbitrary velocity fields in the lower-bound theorem is severely restricted. Although these problems do not provide good examples with respect to application of the lower-bound theorem, the velocity-constraint equations, in many cases, afford exact solutions for materials governed by the nonlinear stress-strain-rate Eqs. 2.

D. Three-bar Truss

Consider a simple truss consisting of three bars of similar material and cross-sectional area A subjected to a vertical load W at point O, as shown in Fig. 9. If the vertical displacement at point O is denoted by u, the axial strains in bars 1 and 2 are given by

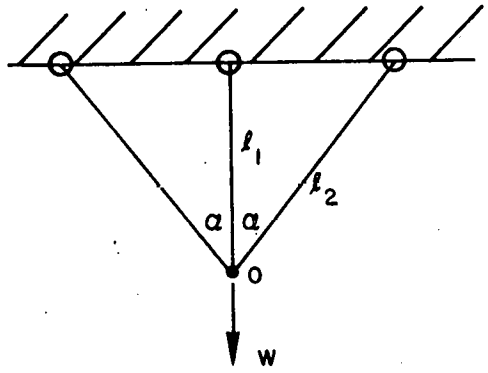

Fig. 9. Three-bar Truss

$$\left.\begin{aligned} \epsilon_1 &= u/\ell_1 \\ \text{and} \\ \epsilon_2 &= (u/\ell_1)\cos^2\alpha \end{aligned}\right\}, \tag{87}$$

and equilibrium requires that the corresponding axial stresses σ_1 and σ_2 satisfy

$$\sigma_1 + 2\sigma_2 \cos\alpha = W/A. \tag{88}$$

The solution for an elastic material is given by

$$\left.\begin{aligned} u &= \frac{W\ell_1}{EA}(1+2\cos^3\alpha)^{-1}, \\ \sigma_1 &= (W/A)(1+2\cos^3\alpha)^{-1}, \\ \text{and} \\ \sigma_2 &= (W/A)\cos^2\alpha(1+2\cos^3\alpha)^{-1}, \end{aligned}\right\} \tag{89}$$

and the solution for steady-state creep defined by the stress-strain-rate Eq. 1 is given by

$$\left.\begin{aligned} \dot{u} &= \dot{\epsilon}_0\ell_1\left(\frac{W}{A\sigma_0}\right)^n\left(1+2\cos^{1+(2/n)}\alpha\right)^{-n}, \\ \sigma_1 &= \left(\frac{W}{A}\right)\left(1+2\cos^{1+(2/n)}\alpha\right)^{-n}, \\ \text{and} \\ \sigma_2 &= \left(\frac{W}{A}\right)\cos^{2/n}\alpha\left(1+2\cos^{1+(2/n)}\alpha\right)^{-n}. \end{aligned}\right\} \tag{90}$$

Assume that an upper bound on the velocity $\dot{u}$ is required. From inequality 15, we obtain

$$\dot{u} \leq \frac{\dot{\epsilon}_0 A \ell_1}{(n+1)\,\sigma_0^n} P^{-1}\left[(\sigma_1^s)^{n+1} + \frac{2}{\cos\alpha}(\sigma_2^s)^{n+1}\right], \tag{91}$$

where σ_1^s and σ_2^s are any stresses satisfying the equilibrium equation

$$\sigma_1^s + 2\sigma_2^s \cos\alpha = \frac{1}{A}\left(\frac{n}{n+1} W + P\right). \tag{92}$$

Consider the class of stress states defined by

$$\sigma_1^s = A^{-1}\left(\frac{n}{n+1} W + P\right)\left[1 + 2\cos^{1+(2/m)}\alpha\right]^{-1},$$

and

$$\sigma_2^s = A^{-1}\left(\frac{n}{n+1} W + P\right)\left[1 + 2\cos^{1+(2/m)}\alpha\right]^{-1} \cos^{2/m}\alpha, \tag{93}$$

which contains the elastic and plastic stress states for $m = 1$ and $m \to \infty$, respectively. Using Eq. 93 in inequality 91, the ratio of the least upper bound to the actual velocity is given by

$$R^+_{m,n} = \frac{1 + 2\cos^{(2/m)(n+1)-1}\alpha}{1 + 2\cos^{1+(2/m)}\alpha}\left[\frac{1 + 2\cos^{1+(2/n)}\alpha}{1 + 2\cos^{1+(2/m)}\alpha}\right]^n. \tag{94}$$

For reference, from Eq. 94, we obtain

$$E^+_n = \frac{1 + 2\cos^{2n+1}\alpha}{1 + 2\cos^3\alpha}\left[\frac{1 + 2\cos^{1+(2/n)}\alpha}{1 + 2\cos^3\alpha}\right]^n, \tag{95}$$

and

$$P^+_n = \frac{1 + \frac{2}{\cos\alpha}}{1 + 2\cos\alpha}\left[\frac{1 + 2\cos^{1+(2/n)}\alpha}{1 + 2\cos\alpha}\right]^n. \tag{96}$$

Figures 10 and 11 show the variation of the upper bound based on the elastic stress state as a function of the creep exponent n and geometry, defined by the truss half-angle α. These data indicate that, in general, the accuracy of the upper bound may be severely dependent on the structure geometry. For a reasonable value of the creep exponent ($n = 7$), the upper bound on the velocity at point O is 1.5 times the actual velocity for a truss with $\alpha = 30°$; for $\alpha = 60°$, the upper bound is about 11 times the actual velocity. Similar results are observed for other values of the creep exponent n.

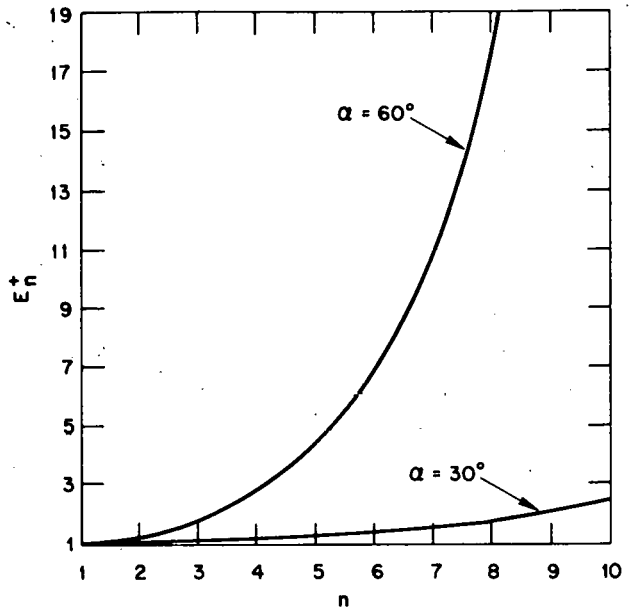

Fig. 10

Least-upper-bound Data for Pressurized Circular Tube Based on Elastic Stresses: Variation of E_n^+ with Creep Exponent n for Truss Half-angles $\alpha = 30°$ and $\alpha = 60°$

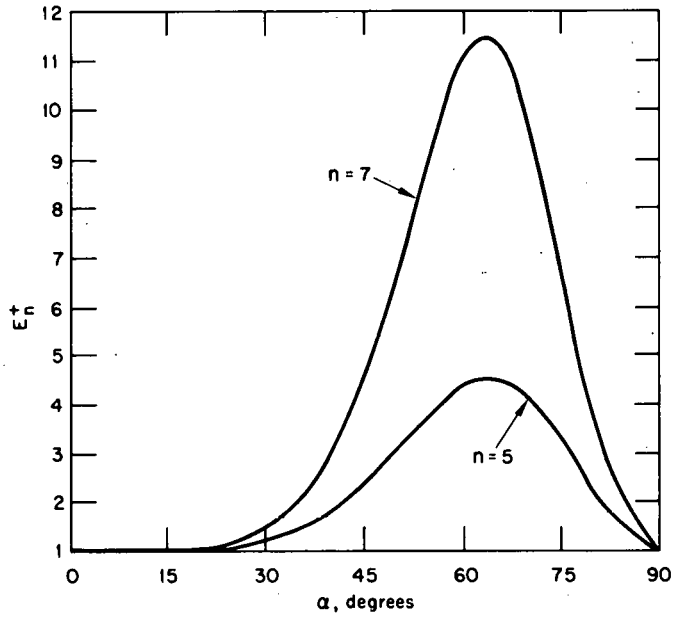

Fig. 11

Least-upper-bound Data for Three-bar-truss Example Based on Elastic Stresses: Variation of E_n^+ with Truss Half-angle α for Creep Exponents n = 5 and n = 7

Figure 12 compares least upper bounds based on the elastic (m = 1) and plastic ($m \to \infty$) stress states for a truss with half-angle $\alpha = 30°$. The upper bound based on the plastic stress state is extremely accurate, with an error less than or equal to 2% over the entire range of n, and is far superior to the upper bound determined by the elastic stress state for values of $n \geq 2$.

Figure 13 compares least upper bounds based on the elastic and plastic stress states as a function of the truss half-angle α for a material with creep exponent n = 7. Except for values of α given approximately by $80° \leq \alpha < 90°$, the bound based on the plastic stress state is preferable. The upper-bound

curve based on the plastic stress state for n = 1 is included to show that, except for α in the range $80° \leq \alpha < 90°$, the bounds based on the plastic state are relatively insensitive to the angle α.

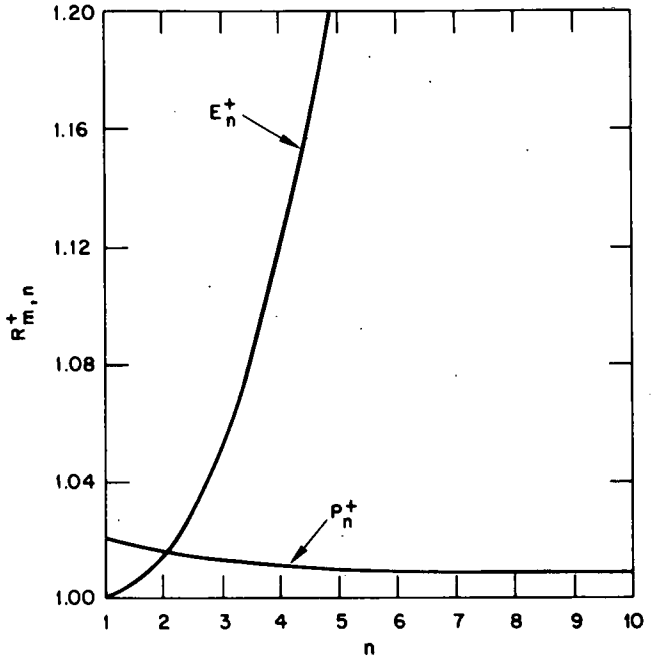

Fig. 12

Least-upper-bound Data for Three-bar-truss Example Based on a Class of Equilibrated Stress Distributions: Variation of $R^+_{m,n}$ with Creep Exponent n for Truss Half-angle $\alpha = 30°$

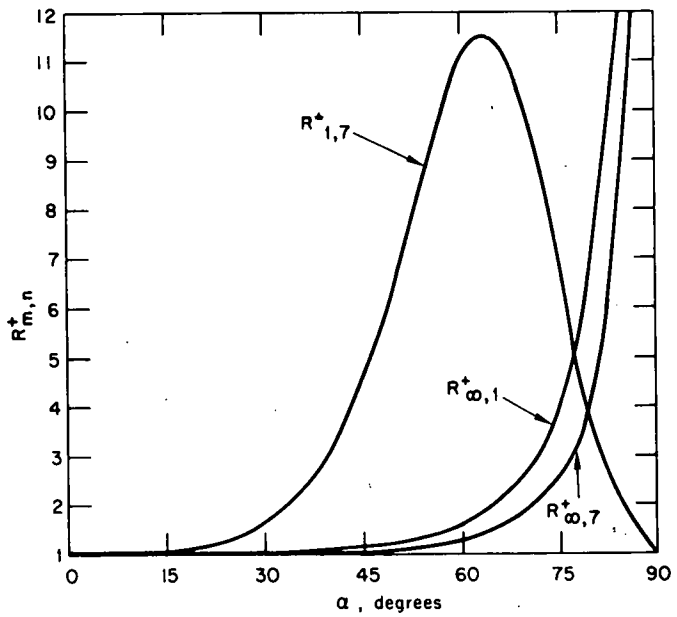

Fig. 13

Least-upper-bound Data for Three-bar-truss Example Based on a Class of Equilibrated Stress Distributions: Variation of $R^+_{m,n}$ with Truss Half-angle α

E. Torsion of a Cylindrical Tube

Consider a circular cylinder of internal and external radii r_i and r_o, respectively, fixed at one end and subjected to a twisting moment M, as shown in Fig. 14. The components of displacement relative to the rectangular coordinate system (x_1,x_2,x_3), with the x_3 axis taken along the axis of the cylinder, are given by

$$\left.\begin{aligned} u_1 &= -\alpha x_2 x_3, \\ u_2 &= \alpha x_1 x_3, \\ \text{and} \\ u_3 &= 0, \end{aligned}\right\} \tag{97}$$

where α is the angle of twist per unit length. The nonzero components of strain are given by

$$\left.\begin{aligned} \epsilon_{23} &= \tfrac{1}{2}\alpha x_1 \\ \text{and} \\ \epsilon_{31} &= \tfrac{1}{2}\alpha x_2 \end{aligned}\right\}, \tag{98}$$

and equilibrium of the cylinder is satisfied in the overall sense, provided the shearing stresses σ_{32} and σ_{31} are such that

$$M = \int_A (x_1\sigma_{32} - x_2\sigma_{31})\, dA. \tag{99}$$

For an elastic material,

$$\left.\begin{aligned} \sigma_{23} &= \mu\alpha x_1 \\ \text{and} \\ \sigma_{31} &= -\mu\alpha x_2 \end{aligned}\right\}, \tag{100}$$

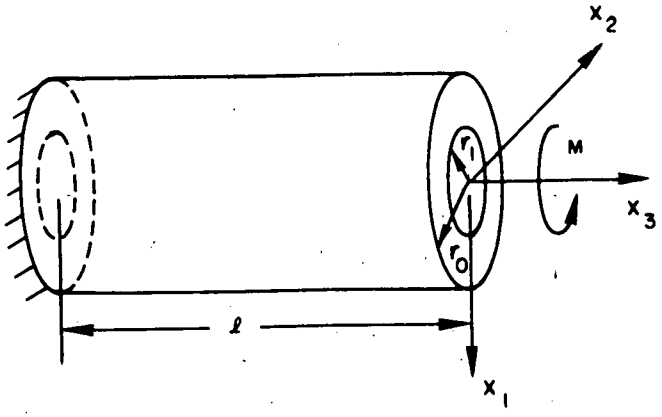

Fig. 14. Circular Tube under Twist

and Eq. 99 is satisfied

$$\alpha = \frac{M}{\mu J_0}, \tag{101}$$

where μ is the elastic shear modulus and

$$J_0 = \frac{\pi}{2}(r_o^4 - r_i^4). \tag{102}$$

Using Eqs. 100 and 101, the resultant shear stress

$$\tau = (\sigma_{32}^2 + \sigma_{31}^2)^{1/2} \tag{103}$$

at any point

$$r = (x_1^2 + x_2^2)^{1/2}$$

is given by

$$\tau = Mr/J_0. \tag{104}$$

Denoting the rate of twist per unit length of the cylinder by $\dot{\alpha}$, the solution for steady-state creep defined by the stress-strain-rate relations of Eq. 2 can be expressed as

$$\tau = \frac{(3 + 1/n)\, Mr^{1/n}}{2\pi\left[r_o^{3+(1/n)} - r_i^{3+(1/n)}\right]} \tag{105}$$

and

$$\dot{\alpha} = \frac{\dot{\epsilon}_0 M^n (\sqrt{3})^{n+1}\, (3 + 1/n)^n}{(2\pi\sigma_0)^n \left(r_o^{3+(1/n)} - r_i^{3+(1/n)}\right)}. \tag{106}$$

Assume that an upper bound on the rate of twist is required. Applying inequality 15, we choose

$$t_i^s = 0 \qquad \left\{\begin{matrix} r = r_i \\ r = r_o \end{matrix}\right\},$$

and

$$t_i^s = \frac{n}{n+1}\, t_i + t_i^* \qquad x_3 = \ell,$$

where t_i^* is some arbitrary additive shear stress. The left-hand side of inequality 15 can then be evaluated as

$$\int_A \left(t_i^s - \frac{n}{n+1}\, t_i\right) \dot{u}_i \, dA = \dot{\alpha}\ell M^*, \tag{107}$$

where M^* represents the added twisting moment.

The effective stress is related to the resultant shear stress by

$$\sigma_e^2 = 3\tau^2, \tag{108}$$

and it follows that

$$\int_V \sigma_{ij}^s \dot{\epsilon}_{ij}^s \, dV = \frac{2\pi \ell \dot{\epsilon}_0 \cdot 3^{(n+1)/2}}{\sigma_0^n} \int_{r_i}^{r_o} (\tau^s)^{n+1} \, r \, dr \tag{109}$$

where τ^s is any equilibrated shear stress due to a twisting moment $[n/(n+1)]\, M + M^*$. Using Eqs. 107 and 108 in inequality 15, we obtain

$$\dot{\alpha} \leq \frac{2\pi \dot{\epsilon}_0 \cdot 3^{(n+1)/2}}{(n+1)\, \sigma_0^n} (M^*)^{-1} \int_{r_i}^{r_o} (\tau^s)^{n+1} \, r \, dr. \tag{110}$$

It may be shown that the ratio of the least upper bound based on the elastic-shear-stress distribution

$$\tau^s = \{[n/(n+1)]\, M + M^*\}\, r/J_0,$$

to the actual rate of twist, is given by

$$E_n^+ = \frac{4}{n+3} \left(\frac{4n}{3n+1}\right)^n \frac{\left[1 - (r_i/r_o)^{n+3}\right] \left[1 - (r_i/r_o)^{3+(1/n)}\right]^n}{\left[1 - (r_i/r_o)^4\right]^{n+1}}. \tag{111}$$

For extremely thin tubes of thickness t, Eq. 111 may be approximated by

$$E_n^+ = 1 + \frac{1}{12}\left(2n^2 - 5n + 4 - \frac{1}{n}\right)(t/r_i)^2 + O(t/r_i)^3. \tag{112}$$

Finally, a class of shear stress distributions is considered that contains the elastic and plastic stress distributions as limiting states. The ratio of the least upper bound to the actual rate of twist is determined as

$$R_{m,n}^+ = \frac{\left(3 + \frac{1}{m}\right)^{n+1} \left(\frac{m}{2m+n+1}\right)}{\left(3 + \frac{1}{n}\right)^n} \cdot \frac{\left[1 - (r_i/r_o)^{(2m+n+1)/m}\right] \left[1 - (r_i/r_o)^{3+(1/n)}\right]^n}{\left[1 - (r_i/r_o)^{3+(1/m)}\right]^{n+1}}. \tag{113}$$

In particular, for the plastic stress state,

$$P_n^+ = \frac{3}{2}\left(\frac{3n}{3n+1}\right)^n \left[\frac{1 - (r_i/r_o)^2}{1 - (r_i/r_o)^3}\right] \left[\frac{1 - (r_i/r_o)^{3+(1/n)}}{1 - (r_i/r_o)^3}\right]^n. \tag{114}$$

The ratio of the upper bound based on the elastic stress distribution to the actual rate of twist is shown in Fig. 15 as a function of the creep exponent n for $r_i/r_o = 0.5$, and in Fig. 16 as a function of r_i/r_o, for several values of the

creep exponent. The bounds are extremely accurate for thin tubes and deteriorate with increasing values of n. Moreover, the overall accuracy of the upper bound based on the elastic stress state is quite reasonable, in comparison with results for other examples considered in Sec. III.

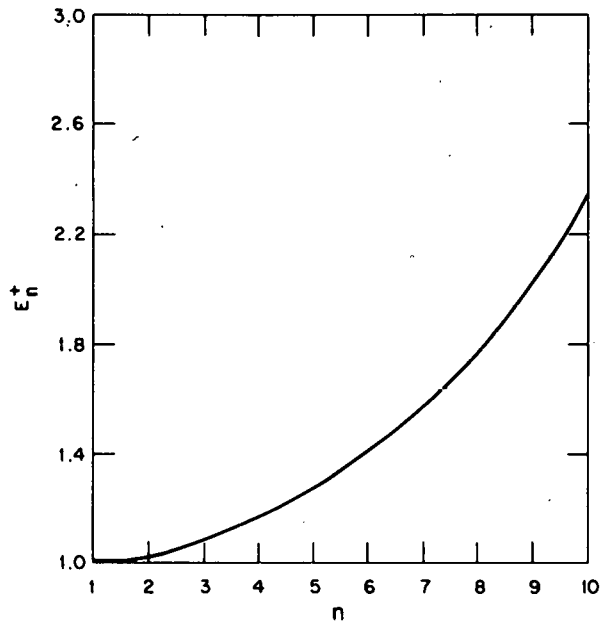

Fig. 15. Least-upper-bound Data for Torsion of a Circular Tube Based on Elastic Stress Distribution: Variation of E_n^+ with Creep Exponent n for a Tube with $r_i/r_o = 0.5$

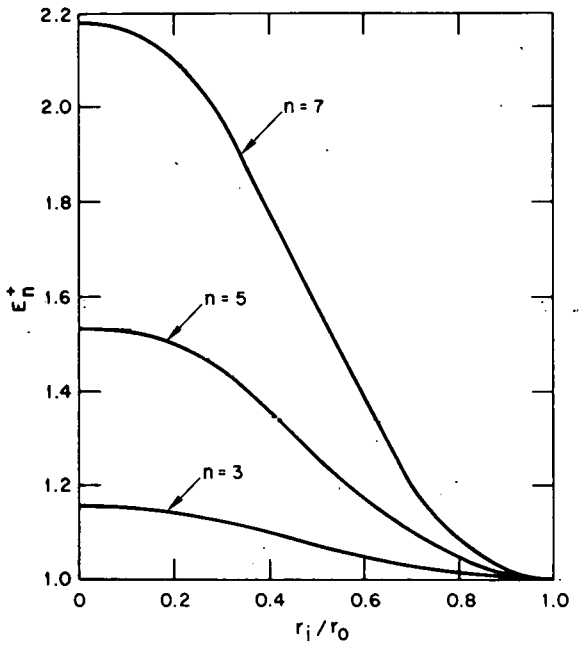

Fig. 16. Least-upper-bound Data for Torsion of a Circular Tube Based on Elastic Stress Distribution: Variation of E_n^+ with r_i/r_o for Several Values of Creep Exponent n

Figure 17 compares upper bounds based on the elastic and plastic stress states, which indicate, as in previous examples, the extreme accuracy of the

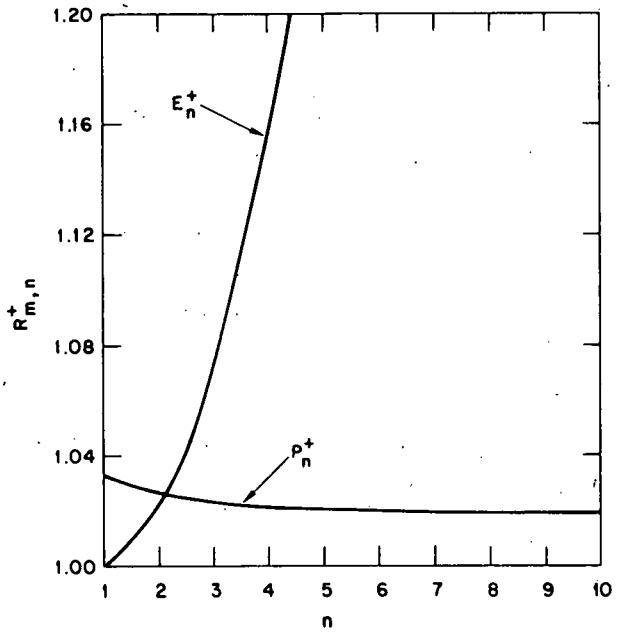

Fig. 17

Least-upper-bound Data for Torsion of a Circular Tube Based on a Class of Equilibrated Stress Distributions: Variation of $R_{m,n}^+$ with Creep Exponent n for $r_i/r_o = 0.5$

bounds based on plastic stresses. Over the range $3 \leq n \leq 9$, the upper bound based on the plastic stress state is about 2% larger than the actual rate of twist.

F. Pressurized Spherical Shell

Consider a spherical shell of arbitrary thickness t, subjected to internal pressure p_i and external pressure p_o, as shown in Fig. 18. Displacement components relative to a spherical coordinate system (r, θ, φ) are denoted by (u,v,w) and, from symmetry,

$$\left.\begin{aligned} &u = u(r) \\ \text{and} \\ &v = w = 0 \end{aligned}\right\}. \tag{115}$$

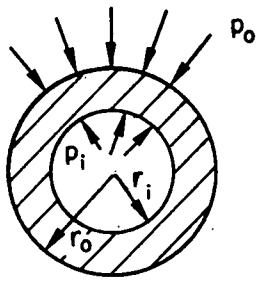

Fig. 18

Pressurized Spherical Shell

The nonzero strain components are given by

$$\left.\begin{aligned} &\epsilon_{rr} = \frac{du}{dr} \\ \text{and} \\ &\epsilon_{\theta\theta} = \epsilon_{\varphi\varphi} = u/r \end{aligned}\right\}, \tag{116}$$

and equilibrium is satisfied, provided the nonzero stress components σ_{rr} and $\sigma_{\theta\theta} = \sigma_{\varphi\varphi}$ are related by

$$\frac{d\sigma_{rr}}{dr} + \frac{2(\sigma_{rr} - \sigma_{\theta\theta})}{r} = 0, \tag{117}$$

in addition to the boundary conditions

$$\left.\begin{aligned} &\sigma_{rr} = -p_i, \quad r = r_i \\ \text{and} \\ &\sigma_{rr} = -p_o, \quad r = r_o \end{aligned}\right\}. \tag{118}$$

The material is assumed to be incompressible; therefore, from Eqs. 116, the radial displacement u must satisfy

$$\frac{du}{dr} + 2\frac{u}{r} = 0. \tag{119}$$

The solution for an elastic material is given by

$$\left.\begin{aligned} u &= \frac{3(p_i - p_o)}{4Er^2}\,\frac{r_i^3 r_o^3}{r_o^3 - r_i^3}, \\ \sigma_{rr} &= A + \frac{B}{r^3}, \end{aligned}\right\} \tag{120}$$

and

$$\left.\begin{aligned} \sigma_{\theta\theta} &= A - \frac{B}{2r^3}, \end{aligned}\right\}$$

where

$$\left.\begin{aligned} A &= -p_i + \frac{r_o^3(p_i - p_o)}{r_o^3 - r_i^3}, \\ B &= \frac{-r_i^3 r_o^3(p_i - p_o)}{r_o^3 - r_i^3}, \end{aligned}\right\} \tag{121}$$

and the solution for steady-state creep, as defined by the stress-strain-rate Eqs. 2, can be written as

$$\left.\begin{aligned} \sigma_{rr} &= A + \frac{B}{r^{3/n}}, \\ \sigma_{\theta\theta} &= \sigma_{\varphi\varphi} = A + \left(1 - \frac{3}{2n}\right)\frac{B}{r^{3/n}}, \end{aligned}\right\} \tag{122}$$

and

$$\left.\begin{aligned} \dot{u} &= \frac{\dot{\epsilon}_0}{2r^2}\left[\frac{3(p_i - p_o)}{2n\sigma_0}\right]^n \frac{r_i^3 r_o^3}{(r_o^{3/n} - r_i^{3/n})}, \end{aligned}\right\}$$

where $\dot{u}$ denotes the radial velocity,

$$A = -p_i + \frac{r_o^{3/n}(p_i - p_o)}{r_o^{3/n} - r_i^{3/n}},$$

and

$$B = -(p_i - p_o)\frac{r_i^{3/n} r_o^{3/n}}{r_o^{3/n} - r_i^{3/n}}. \qquad (123)$$

Assume that an upper bound on the radial velocity at the inner surface $r = r_i$ is required. Following the procedure used for the pressurized cylindrical tube, the ratio of the least upper bound based on elastic stresses to the actual radial velocity at $r = r_i$ is determined as

$$E_n^+ = n^{n-1}\frac{1 - (r_i/r_o)^{3n}}{1 - (r_i/r_o)^3}\left[\frac{1 - (r_i/r_o)^{3n}}{1 - (r_i/r_o)^3}\right]^n, \qquad (124)$$

which for thin shells has the expansion

$$E_n^+ = 1 + \frac{3(n-1)^2(n+1)}{8n}(t/r_i)^2 + O(t/r_i)^3. \qquad (125)$$

For the class of equilibrated radial stress distributions

$$\sigma_{rr}^s = A_m + B_m r^{-3/m}, \qquad (126)$$

with the constants A_m and B_m determined from Eqs. 118, we obtain

$$R_{m,n}^+ = \frac{1}{m - n - 1}\left(\frac{n}{m}\right)^n\left(r_o^{3/n} - r_i^{3/n}\right)^n \frac{r_o^{(3/m)(m-n-1)} - r_i^{(3/m)(m-n-1)}}{r_i^3 r_o^3}$$

$$\cdot\left(\frac{r_i^{3/m} r_o^{3/m}}{r_o^{3/m} - r_i^{3/m}}\right)^{n+1}. \qquad (127)$$

For the plastic stress state, we obtain, from Eq. 127,

$$P_n^+ = \lim_{m\to\infty} R_{m,n}^+ = \frac{-\frac{1}{3}[1 - (r_i/r_o)^3]}{(r_i/r_o)^3 \ln(r_i/r_o)}\left(\frac{-\frac{n}{3}[1 - (r_i/r_o)^{3/n}]}{\ln(r_i/r_o)}\right)^n. \qquad (128)$$

Figure 19 shows the dependence of E_n^+ on the creep exponent n for a sphere with $r_i/r_o = 0.5$. Again, the accuracy of the upper bound diminishes rapidly for large values of n. Figure 20 gives the variation of E_n^+ with r_i/r_o for several values of n, and it appears that reasonably accurate upper bounds based on elastic stresses are obtained only for thin shells.

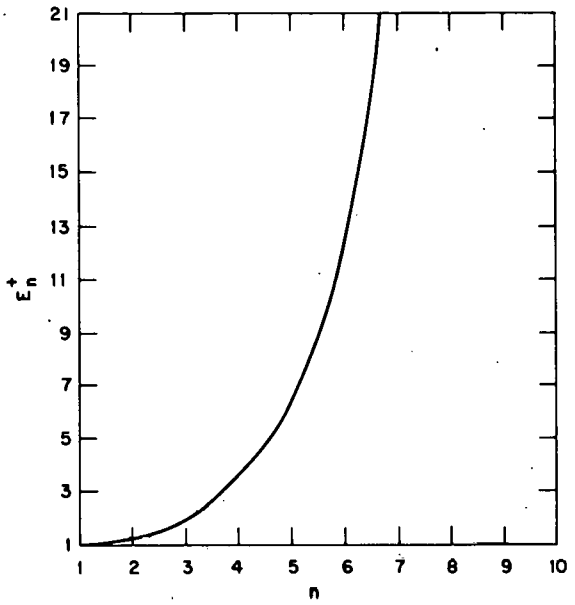

Fig. 19. Least-upper-bound Data for Pressurized Spherical Shell Based on Elastic Stress Distribution: Variation of E_n^+ with Creep Exponent n for a Shell with $r_i/r_o = 0.5$

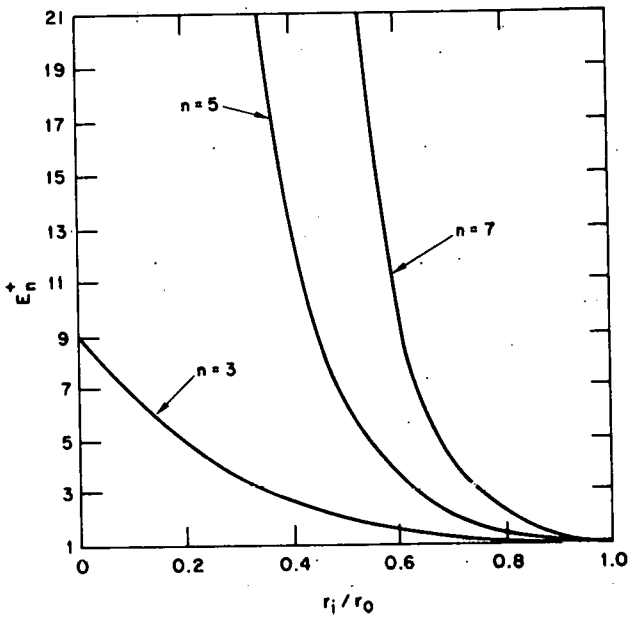

Fig. 20. Least-upper-bound Data for Pressurized Spherical Shell Based on Elastic Stress Distribution: Variation of E_n^+ with r_i/r_o for Several Values of Creep Exponent n

Figure 21 compares bounds based on the elastic and plastic stress states for a sphere with $r_i/r_o = 0.5$, and it is evident, as with the previous examples, that the plastic stress state leads to upper bounds that are extremely accurate compared with those based on the elastic stress state.

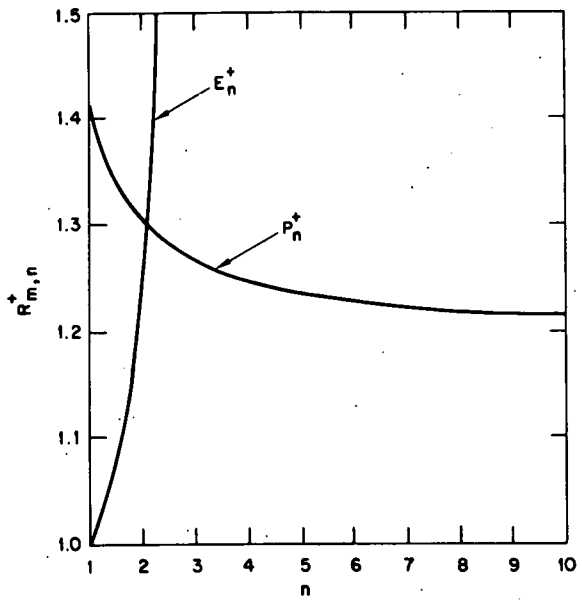

Fig. 21

Least-upper-bound Data for Pressurized Spherical Shell Based on a Class of Equilibrated Stress Distributions: Variation of $R_{m,n}^+$ with Creep Exponent n for a Shell with $r_i/r_o = 0.5$

IV. APPLICATION OF BOUNDING THEOREMS TO COMPLEX STRUCTURES

Application of the upper- and lower-bound displacement-rate theorems to complex structures requires the determination of an appropriate equilibrated stress distribution σ_{ij}^s, and a consistent velocity field $\dot{u}_i^c$. Since the objective is to obtain close upper and lower bounds and thereby provide an accurate estimate of the true displacement rate, it is necessary to develop general methods for constructing the fields σ_{ij}^s and $\dot{u}_i^c$ to yield bounds of specified quality. Unfortunately, these general methods have yet to be developed.

Due to the enormous capability of the finite-element method as applied to elastostatic analysis, a logical starting point is the use of the elastic solution state for the required quantities σ_{ij}^s and $\dot{u}_i^c$. The vast majority of engineering problems in the domain of elastic structural analysis can be solved accurately and economically through the use of finite-element techniques. Without going into unnecessary details at this point, it should be clear that results for the elastic stress and displacement fields obtained through use of the finite-element method must be regarded as approximate and may not always exactly satisfy the stated requirements for σ_{ij}^s and $\dot{u}_i^c$. This does not appear to be a serious disadvantage and simply means that we must be satisfied with approximate determinations of upper and lower bounds. The usefulness of this approach can be established only through applications and suitable computer experiments.

The basic procedure will be demonstrated for the upper-bound theorem, as represented by the inequality 17. The original structure of volume V is subdivided into N regions or elements of volume V_j, and inequality 17 is replaced with

$$\dot{u} \leq \frac{\dot{\epsilon}_0}{\sigma_0^n (n+1)} P^{-1} \sum_{j=1}^{N} \int_{V_j} (\sigma_e^s)_j^{n+1} \, dV_j. \tag{129}$$

A value of the added load P is selected and a finite-element solution is generated for the appropriately modified boundary conditions, as discussed in Sec. II. The approximate value of the effective elastic stress so obtained is denoted by $\hat{\sigma}_e$. Substituting $\hat{\sigma}_e$ for σ_e^s in inequality 129, an approximate determination of an upper bound for $\dot{u}^*$ is established for the given choice of the the added load P. The process is then repeated for several other values of P in order to determine a "best" upper bound. Three or four calculations with different values of the added load P should be sufficient to obtain a reasonable estimate of the minimum upper bound.

The above method has been successfully applied to the cantilever-beam and pressurized-cylindrical-tube examples discussed in Sec. III. Results for the pressurized-tube problem are summarized below. A thick cylindrical tube subjected to internal pressure was modeled with 12 constant-strain quadrilateral ring elements as shown in Fig. 22.

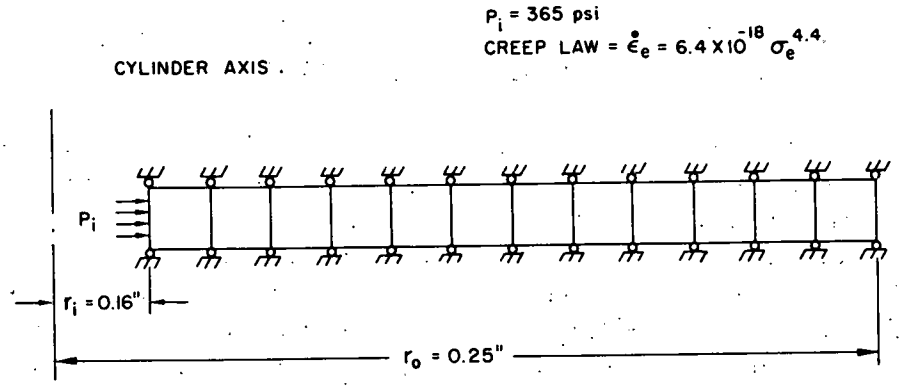

Fig. 22. Finite-element Idealization of a Thick-walled Cylinder

The finite-element program AXICRP[10] was used to generate the elastic solution for the optimum value of the added pressure $p^* = p_i/(n+1)$. An upper bound on the velocity at the inner surface, $\dot{u}(r_i)$, was computed using inequality 129. For this problem, inequality 129 can be expressed as

$$\dot{u}(r_i) r_i \sigma_0^n \le \frac{1}{p_i} \sum_{j=1}^{12} (\hat{\sigma}_e)_j^{n+1} \frac{r_j^2 - r_{j-1}^2}{2}, \tag{130}$$

where $(\hat{\sigma}_e)_j$ is the effective elastic stress in element j; r_{j-1} and r_j denote, respectively, the inner and outer radii of element j; and for convenience we have taken $\dot{\epsilon}_0 = 1$. The right-hand side of inequality 130 was evaluated for several values of the creep exponent; the results are summarized in Table I.

TABLE I. Comparison of Analytical and Finite-element Upper Bounds

	$\dot{u}(r_i) r_i \sigma_0^n$		E_n^+	
n	Exact	Upper Bound Using AXICRP	Analytical	AXICRP
1	23.74	24.25	1.00	1.02
3	121.7×10^5	147.7×10^5	1.18	1.21
4.4	119.5×10^9	185.4×10^9	1.50	1.55

The "exact" result is determined from Eqs. 72 and 73, and the upper bound using AXICRP is determined from inequality 130. The analytical evaluation of inequality 17 based on the elastic stress state, and the upper bound based on AXICRP, are then used to compute the comparable values of E_n^+, which is the ratio of the upper bound to the exact solution of the problem. The small differences in the E_n^+ results between exact and finite-element evaluation of the bound indicate that the use of the finite-element method does not lead to any appreciable deterioration of the bound.

Using the complete AXICRP solution for the pressurized circular cylinder shown in Fig. 22, an upper bound on the radial velocity at the inner surface of the cylinder was calculated using the computed stress distribution at various times during the stress-redistribution process from the initial elastic to final stationary state. The ratio of the upper bound based on the stress state at time t to the actual velocity in the stationary state for times $t \geq t_{ss}$, where t_{ss} denotes the time required to achieve a stationary state, is denoted by R^+ and is shown in Fig. 23 as a function of the dimensionless time $\tau = t/t_{ss}$.

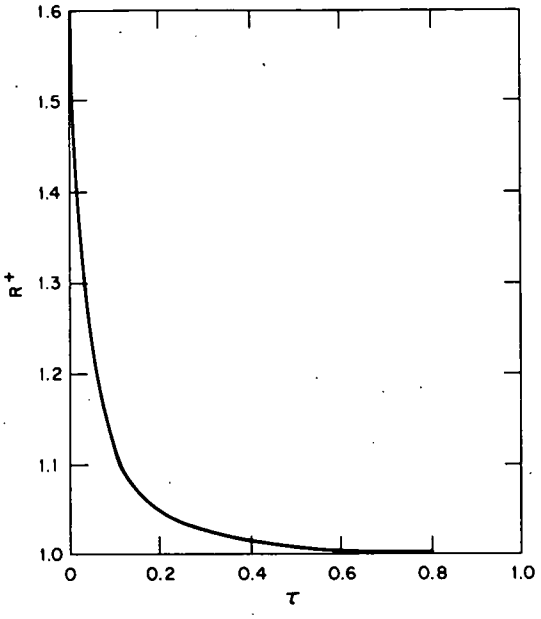

Fig. 23. Figure-of-merit Measuring Approach to Steady-state Upper Bound as a Function of Dimensionless Time to Steady State

These results illustrate the rapid improvement in accuracy of the upper bound, based initially on the elastic state, during the early stages of the stress-redistribution process. For the class of equilibrated stress states generated from elastic to steady-state creep behavior, small deviations from the elastic stress distribution $\hat{\sigma}^s_{ij}$, such that the integral $\int_V (\hat{\sigma}^s_e)^{n+1}\, dV$ is reduced in value, lead to large increases in the accuracy of the upper bound determined by inequality 17. Although this result is strictly applicable to the sequence of stress distributions obtained with the AXICRP code, it provides an incentive for the development of numerical procedures to obtain equilibrated stress states that represent small variations from the elastic state but lead through inequality 17 to the determination of extremely accurate upper bounds. The fact that relatively small adjustments in the stress distribution provide large improvements in the bound leads one to believe that any automated search procedure for bound minimization would be numerically stable and that "convergence" in a practical sense would be very rapid.

V. CONCLUSIONS

This report describes an initial effort in the area of bounding and approximation methods for inelastic analysis. The evaluation of surface-velocity bounding theorems for steady-state creep deformation has been considered, and the accuracy of these bounding theorems based on elastic- and plastic-solution states for several simple structures has been established.

For the several examples considered, upper bounds based on the plastic stress state were remarkably accurate. However, the determination of the plastic stress state at collapse is a formidable problem; for even relatively simple structures, only a few solutions have been obtained at present. On the other hand, deformation-rate bounds based on the elastic stress state can be easily obtained for most structures through the use of standard finite-element techniques. These bounds were rather inaccurate for certain structures and for relatively large values of the creep exponent ($n > 10$). For materials having creep exponents on the order of $n = 4$ or $n = 5$, the results provided reasonable bounds for most values of the geometric parameters.

The potential value of the bounding theorems as a general-purpose design tool depends on the development of automated procedures for application to arbitrary structures. Further, it is necessary that these procedures give accurate bounds for relative small expenditures of computing effort. The example presented in Sec. IV indicates that such a method, based on the finite-element method, can be developed. It seems desirable to first develop these procedures for basic structural elements such as beams, plates, and shells. The result would be a readily usable tool for accurately estimating surface velocities for these basic structures in a state of steady creep. This should be possible for a fraction of the cost of generating the complete steady-state creep solution, since only a few elastic finite-element computations should be needed.

Finally, the numerical procedures developed for calculating velocity bounds for steady-state creep behavior can be used to determine appropriate equilibrated stress and consistent velocity fields for bounding theorems applicable to other forms of inelastic material response.

REFERENCES

1. J. B. Martin, *A Note on the Determination of an Upper Bound on Displacement Rates for Steady Creep Problems*, J. Appl. Mech. *33*(1), 216-217 (Mar 1966).

2. A. C. Palmer, *A Lower Bound on Displacement Rates in Steady Creep*, J. Appl. Mech. *34*(1), 216-217 (Mar 1967).

3. F. A. Leckie and J. B. Martin, *Deformation Bounds for Bodies in a State of Creep*, J. Appl. Mech. *34*(2), 411-417 (June 1967).

4. F. A. Leckie and A. R. S. Ponter, *Deformation Bounds for Bodies Which Creep in the Plastic Range*, J. Appl. Mech. *37*(2), 426-430 (June 1970).

5. A. R. S. Ponter and F. A. Leckie, *The Application of Energy Theorems to Bodies Which Creep in the Plastic Range*, J. Appl. Mech. *37*(3), 753-759 (Sept 1970).

6. A. R. S. Ponter, *Deformation, Displacement, and Work Bounds for Structures in a State of Creep and Subject to Variable Loading*, J. Appl. Mech. *39*(4), 953-958 (Dec 1972).

7. J. B. Martin, *A Displacement Bound Technique for Elastic Continua Subjected to a Certain Class of Dynamic Loading*, J. Mech. Phys. Solids *12*(3), 165-175 (June 1964).

8. D. C. Drucker, *A More Fundamental Approach to Plastic Stress-Strain Relations*, Proceedings, First U.S. National Congress of Applied Mechanics, ASME, pp. 487-491 (1952).

9. R. K. Penny and D. L. Marriott, *Design for Creep*, McGraw-Hill, New York (1971).

10. W. H. Sutherland, *A Finite Element Computer Code (AXICRP) for Creep Analysis*, BNWL-1142 (Oct 1969).

11. R. Hill, *New Horizons in the Mechanics of Solids*, Mech. Phys. Solids *5*, 66-74 (1956).